energy&fuels

pubs.acs.org/EF
Article

Persistent CO_2 Reduction Performance of an Ag Nanoparticle Gas Diffusion Electrode in Realistic Dynamic PV-Driven Operation

Thérèse Cibaka, Tsvetelina Merdzhanova,* Oleksandr Astakhov, Sergey Shcherbachenko, Guangxin Liu, Chuyen van Pham, Uwe Rau, and Peter Strasser

Cite This: *Energy Fuels* 2025, 39, 22776–22783

ABSTRACT: Progress in the development of CO_2 reduction catalysts has revealed more stable and selective options for solar fuel production. In most cases, the catalysts are tested under steady-state conditions. However, to become a reliable long-term storage solution for renewable energy, particularly photovoltaics (PV), CO_2 electroreduction must tolerate power intermittency. Direct coupling of CO_2 electrolyzers to PV devices enables carbon utilization and efficient energy storage but requires catalysts that maintain consistent performance under dynamic power input. Herein, we select an Ag nanoparticle gas diffusion cathode with stable CO production across a wide current density range. The system, directly coupled to a hardware-emulated Si-PV module operating under a realistic sunny day profile, achieves 96% energy coupling efficiency and reaches a cumulative solar-to-chemical (CO) efficiency of 8.8% in 1 day. This study demonstrates the potential of Ag-based cathodes for robust performance in variable PV-powered systems and introduces a novel test methodology that better reflects real-world PV-electrolyzer integration, thereby advancing practical implementation of solar-driven CO_2 reduction.

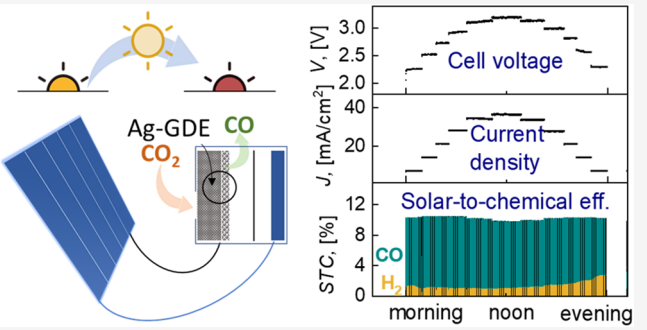

1. INTRODUCTION

Two major renewable energy sources, wind and solar, constitute 63% of the global renewable power capacity.[1] More specifically, the solar market is growing at a faster rate than initially predicted, thereby making a significant contribution to the green energy transition.[2] However, the efficient use of photovoltaic (PV) capacity is limited by the temporal mismatch between generation and demand, while power intermittency hinders grid compatibility. The optimal use of PV energy requires an energy storage strategy, particularly on a long timescale, to address seasonality. An ideal storage solution effectively absorbs intermittent DC power from PV generation while maintaining consistent performance across a broad dynamic range. In view of multiterawatt-scale PV generation, any PV-storage solution must utilize abundant materials and up-scalable synthesis methods.

The conversion of rampant CO_2 into fuels or valuable chemicals through the electrochemical CO_2 reduction reaction (CO_2RR) presents a high-potential strategy for energy storage and carbon utilization when powered by renewable energy, such as PV. For this purpose, catalysts used in electrochemical cells (ECs) must handle intermittent power input and industrially relevant current densities (>200 mA/cm^2) while maintaining high selectivity toward target products.[3] The realistic intermittent operating context of PV storage has been largely neglected in catalyst development and testing. The reported catalysts often have a narrow window of operating voltages with high faradaic efficiency toward the target product.[4,5]

Our previous works have demonstrated the self-sustained operation and high performance of PV coupled with batteries,[6,7] ECs,[8,9] and their combinations.[10,11] Connecting PV and EC systems without full integration allows independent optimization and preserves device integrity. Direct coupling also enables the on-site use of PV-generated DC power for solar fuel production, thereby alleviating grid congestion. At the laboratory scale, solar-to-chemical efficiency (*STC*) or the ratio of solar energy irradiated on the exposed area of PV converted into chemicals by EC is the highest for direct-coupled PV-EC devices.[12−18] The high performance of these systems is based on matching the PV and EC current voltage characteristics in such a way that their intersection, the operating point (OP) of the PV-EC device, is in a close vicinity to the maximum power point (MPP) of the PV device. The proximity of the OP to the MPP or the degree of power

Received: July 15, 2025
Revised: September 12, 2025
Accepted: September 15, 2025
Published: September 24, 2025

https://doi.org/10.1021/acs.energyfuels.5c03523
Energy Fuels 2025, 39, 22776−22783

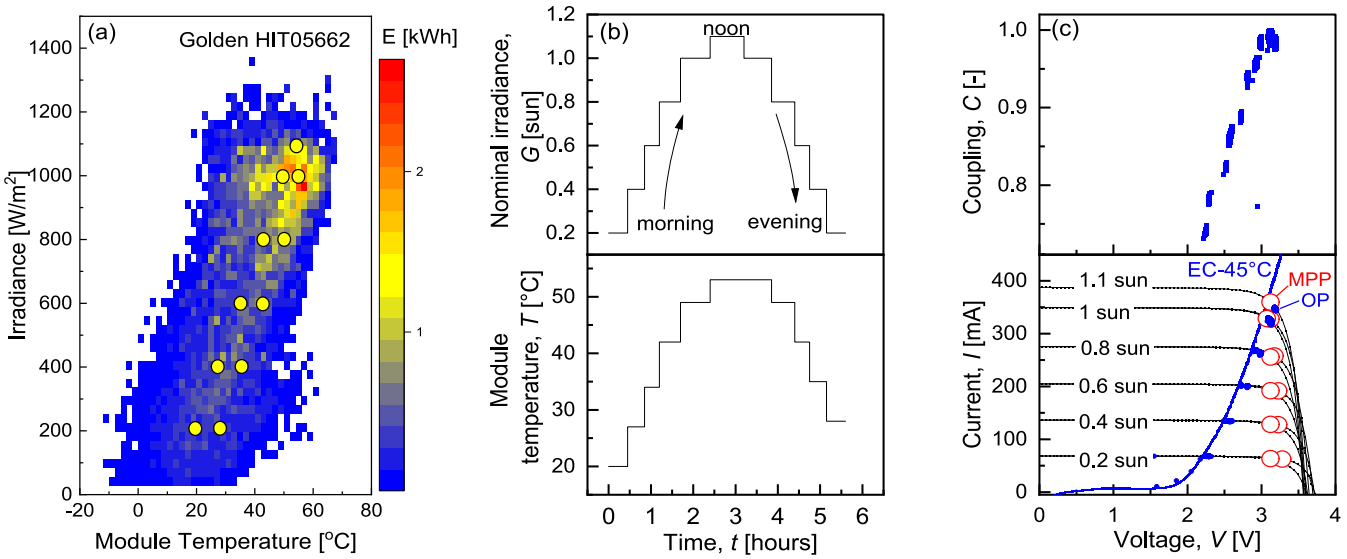

Figure 1. (a) Maximum yearly cumulative energy of an SHJ PV module in Golden plotted against irradiance and temperature conditions. The yellow circles indicate 11 representative irradiance and temperature combinations of a summer day. (b) Eleven dynamic nominal irradiance and module temperature conditions simulating a single summer day condensed in 5 h. (c) Bottom section: EC polarization curve crossing PV−I−V characteristics under the 11 representative G and T conditions. The PV-EC operating points are recorded as blue points on the PV−I−V curve, and MPPs are represented as red hollow circles. Upper section: PV-EC power coupling at each V_{OP} during a single day's operation.

coupling is quantified using the power coupling factor (or power coupling efficiency).[19−21] In the case of intermittent power input, the power coupling factor, which represents a specific moment in time, is not always an adequate metric for evaluating the coupling performance over a period of operation. Therefore, it is useful to evaluate the energy coupling factor, which is the ratio of the energy utilized by the EC to the maximum energy that the PV device could deliver over the same period.

CO_2 reduction catalysts in directly coupled PV-EC systems are typically tested under fixed lab conditions of PV (1 sun, AM 1.5G, 25 °C),[8,9,12−18,22] where the optimization of PV-EC power coupling is straightforward. In reality, the PV current−voltage (I−V) output characteristics vary with the irradiance (G) spectrum and module temperature (T),[23−27] shifting both the operating and maximum power points. This has two major implications: the variation in PV-EC power coupling efficiency and the variation in the catalyst behavior in terms of selectivity and potential stability. In our work, we address both aspects. We studied the behavior of a silver catalyst optimized for a broad dynamic range of operating conditions in a PV-EC system, optimized for high power and energy coupling efficiency in dynamic operation.

Silver is a relatively abundant catalyst with high CO selectivity, making it a strong candidate for large-scale CO_2RRs. This work employs an in-house developed Ag nanoparticle gas diffusion electrode (Ag-GDE)[28] for testing as a CO-selective cathode with a variable PV power input. The Ag gas diffusion electrode (GDE) was fabricated via a scalable industrial method, doctor blading, of custom silver ink onto a gas diffusion layer. The ink was optimized for uniform coating and achieved approximately 94% CO selectivity across 50−200 mA/cm^2.[29] The Ag-GDE cathode, the focus of our study, was tested in a full-flow CO_2RR electrochemical cell using IrO_x as the benchmark anode due to its high activity and low overpotential. However, for practical implementation, more affordable and earth-abundant alternatives are needed. While the oxygen evolution reaction is sluggish, the ethylene glycol oxidation reaction driven by noble-metal-free catalysts like NiFe LDH offers lower oxidation potentials at the anode,[30] thereby increasing the overall cell voltage efficiency and STC_{CO}. In this study, we selected a well-established reference anode material (IrOx) and reaction (OER) as reference points to maintain focus on the Ag-GDE and facilitate a comparison with previously reported work.

To study the interplay of the electric characteristics of PV and EC devices under realistic but reproducible and well-controlled conditions, we employed a novel high-precision PV emulation device dedicated to this type of study.[31] Via the emulation of PV IVs, any realistic irradiance and temperature scenarios for PV output can be tested with high reproducibility. The output of a state-of-the-art silicon heterojunction (SHJ) or Si−PV module with 23.8% efficiency (1 sun AM 1.5G and 25 °C) was emulated for a typical sunny day (sunrise to sunset) in Golden (Colorado, USA) in a stepwise profile for irradiance from 0.2 to 1.1 to 0.2 sun and temperatures from 20 to 53.5 °C. The same "day" was repeated three times in the experiment. The PV-EC device performance was assessed via the power and energy coupling factor, while the Ag-GDE was evaluated for product selectivity, stability, and solar-to-chemical efficiency. The results highlight the strong potential of the Ag-GDE for efficient CO_2 reduction and solar energy storage in direct-coupled PV-EC systems.

2. RESULTS AND DISCUSSION

2.1. Realistic Irradiance, Temperature Profile, and PV-EC Current−Voltage Electric Interplay. For ambient conditions and test scenarios, we relied on the widely used NREL data set for PV modules operating in Golden, Colorado (USA).[32] To maximize PV energy utilization, the PV-EC power coupling efficiency must be optimized to the irradiance (G) and temperature (T) ranges corresponding to the maximum energy yield of the specific PV installation. Figure 1a shows the cumulative yearly energy output of an SHJ PV module in Golden, Colorado, as a function of G and T. The

https://doi.org/10.1021/acs.energyfuels.5c03523
Energy Fuels 2025, 39, 22776−22783

energy peaks at 1 sun and 49 °C. The yellow circles mark 11 representative $G-T$ pairs simulating a typical high-output day, forming a time series from 0.2 sun−20 °C to 1.1 sun−53.5 °C and back, condensed into a 5-h profile (Figure 1b). The morning and afternoon irradiance profiles are symmetric, peaking at 1.1 sun, with higher afternoon temperatures due to ambient warming. Figure 1c displays the PV IV curves of an SHJ module emulated in this work under these 11 $G-T$ conditions (Table M1 in the Method Section-Supporting Information), scaled to match the EC polarization curve presented in blue. As the irradiance increases, the PV current at the maximum power point (I_{MPP}) also increases.

At equal irradiances but higher temperatures (afternoon), the current−voltage curves shift to lower voltages, with V_{MPP} decreasing, as is typical for most solar cells.[27] Separate effects of temperature and irradiance on PV $I-V$s are available in Supporting Information (Figure S1). The current output of PV increases with irradiance from 67 mA at 0.2 sun to 360 mA at 1.1 sun, while the EC operating voltage increased from 2.23 to 3.2 V, as presented in Figure 1c.

In order to achieve optimal PV-EC power coupling under peak irradiance conditions (1.1 sun, 53.5 °C), the PV characteristics in Figure 1c are scaled for the PV emulator to reproduce the IVs of a five-cell serially connected PV module with a PV-to-EC area ratio of 4.7. PV-EC scaling defines the device's operating power range and is critical for techno-economic feasibility. Higher PV-to-EC area ratios (A_{PV}/A_{EC}) are usually more economically favorable. One of the main contributors to EC cost is the electrode materials.[33] The use of abundant materials is a determinant to insert PV-EC as a commercially competitive, sustainable, and resilient solution. The silver load of our cathode was 2 mg/cm^2, which at an area ratio of 4.7 corresponds to the use of approximately 4.3 g of silver in EC per m^2 of the Si-PV module to realize CO_2 reduction storage. This is a significant amount compared to the Ag use in modern Si-PV panels, which ranges from approximately 0.3 to 0.5 g/m^2.[34] Further development, such as improving the electrochemical cell design to boost the current density at a low overpotential, is likely to increase the $A_{PV}/A_{EC\ ratio}$.

The PV-EC power coupling at each V_{OP} is shown in the upper part of Figure 1c. The power coupling in the system remains above 0.70 at all V_{OP}, peaking at 0.98−1 at the highest irradiances, where coupling losses can be most critical.

2.2. Performance of the Ag-GDE in PV-EC under Realistic Triple Sunny Day Conditions. The Ag-GDE performance under variable power input was evaluated via PV-EC operation over three identical 5-h simulated days, separated by 30 min night phases, compressing the full experiment into a 16 h period. The temporal evolution of PV-EC operation over 13 h of nonaccelerated daytime and 20 min of highly accelerated daytime is presented in Supporting Information (Figures S2 and S3) and demonstrates that the system can withstand multiple daily fluctuations while maintaining a reproducible power coupling efficiency, stable current−voltage behavior, and consistent CO selectivity. In Figure 2a, we present the temporal evolution of the operating voltage and current density (V_{OP} and J_{OP}) of the EC, PV-EC power coupling factor C, faradaic efficiency (FE) of the products, and solar-to-chemical efficiency (STC). Under day-and-night G and T cycling conditions, PV-EC maintained reproducible V_{OP} and J_{OP}, and significant power coupling efficiency, demonstrating Ag-GDE stability over the course of 16 h operation with a fluctuating power input. SEM images of fresh and used Ag-GDEs (Figure S4, Supporting Information) show that, after extended operation, some Ag particles appear to have fused together, but no changes in the operating current density were observed. Further investigation is required to determine the cause and implications of this morphological change.

The available PV power output is primarily affected by irradiance. As a result, V_{OP} and J_{OP} in Figure 2a followed the irradiance pattern in Figure 1b. Throughout the simulated day, the PV maximum power ($P_{MPP} = V_{MPP} \times I_{MPP}$) ranged between 200 and 1200 mW, and our system maintained a power coupling factor between 0.73 (in the mornings) and 1 (around noon). This result is comparable to the power efficiency profiles of maximum power point trackers for a similar range of power,[35] highlighting the relevance of direct coupling, particularly when operating across a broad range of power values.

In Figure 2a, the Ag-GDE exhibited a total FE (CO and H_2) of approximately 100% on day 1, 97 and 94% on day 2 and day 3. The CO faradaic efficiency remained consistently higher than that of H_2 throughout the simulated triple-day. Overall, Ag-GDE in our PV-EC system favored CO_2RR over HER across the full EC current density range (7−37 mA/cm^2), indicating the high potential of the Ag cathode for PV storage applications.

Up to the third hour of operation on day 1, and independent of V_{OP} and J_{OP} fluctuations, both FE_{CO} and FE_{H2} remained at 86 and 14%, respectively. In general, FE_{H2} typically increases at a low overall cell voltage.[4,36−38] In this study, this refers to the morning and evening. However, on day 1, the cathode is highly CO-selective, and the increase in H_2 evolution at a lower cell voltage in the morning is suppressed. Toward the evening, after 4 h of operation, when the cell voltage is lower again, the CO selectivity is somewhat reduced but still predominant.

We attribute this behavior to the use of a freshly prepared, highly hydrophobic Ag-GDE, which effectively inhibits the electrolyte (1M, $KHCO_3$)−catalyst interaction. However, over time, the presence of ions such as OH^-, HCO_3^-, and K^+, and possible salt precipitation can decrease the hydrophobicity of the fresh Ag-GDE and presumably allow more electrolyte into the triple-phase boundary, increasing H_2 formation as a result of water reduction.[39,40] The decrease in hydrophobicity was confirmed by the presence of electrolyte-derived potassium structure in the cross section of Ag-GDE and by a reduction in the contact angle between a water droplet and Ag-GDE surface, decreasing from 146° for the fresh Ag-GDE to 133° after 1 day of operation, and further to 116° after 3 days. The corresponding contact angle measurements and EDX maps of the cross section of the used Ag-GDE are shown in Figures S5 and S6, respectively, in the Supporting Information.

At the beginning of day 2, the Faradaic efficiency toward CO was higher than that at the end of day 1, despite operating at a similar voltage range. Multiple parameters are likely to affect selectivity, such as the hydrophobicity of Ag-GDE, HCO_3^- availability, structural changes in silver nanoparticles, insertion of K^+ species in the surface and cross section of Ag-GDE, etc. We suggest that this improvement is related to the electrolyte refreshment carried out prior to day 2, which appears to enhance CO_2 reduction selectivity. A similar trend can be observed in Figure S8 of the Supporting Information for the experiment conducted at a constant voltage of 3.0 V, where an electrolyte refreshment after 5 h led to improved CO

https://doi.org/10.1021/acs.energyfuels.5c03523
Energy Fuels 2025, 39, 22776−22783

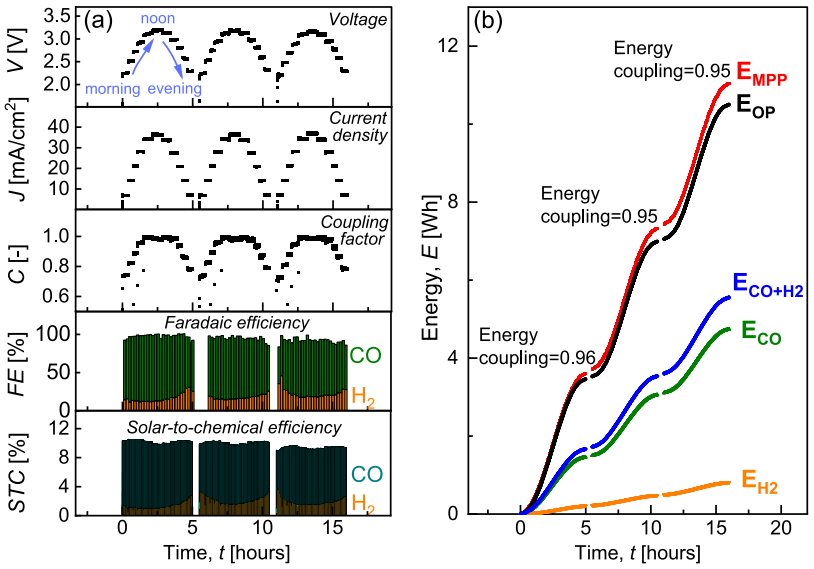

Figure 2. (a) Temporal evolution of PV-EC operating voltage and current density, power coupling factor of PV-EC, and faradaic efficiencies at operating points during a simulated accelerated triple-day. (b) Cumulative energies involved in each step of the solar-to-chemical conversion efficiency during the triple-day and daily energy coupling.

selectivity. At the beginning of day 3, after a total of 10 h of operation, no improvement in CO selectivity was observed compared to the night of day 2, despite the electrolyte refreshment. Presumably, the effects of the refreshment were overpowered by another time-dependent effect, such as structural changes in the GDE.

On day 2 and predominantly on day 3, Ag-GDE showed higher CO selectivity at elevated V_{OP}, coinciding with peak irradiance or "*near noon*" when PV-EC power and *C* were highest. The *STC* values remained at approximately 10% throughout the course of the triple-day experiment. STC_{CO} and STC_{H2} during the days followed the pattern of FE_{CO} and FE_{H2}.

Figure 2b shows the PV-EC performance as cumulative energy over the "triple-day," with reproducible energy coupling factors of 0.96, 0.95, and 0.95 for the three identical days. Power coupling captures the performance at a specific moment in time, whereas energy coupling represents the cumulative fraction of extractable PV energy delivered to the EC system over a given period. In practical applications with intermittent PV outputs, energy coupling serves as a more relevant metric over extended durations.

Table 1 presents a summary of the total solar-to-chemical efficiencies and *STC* toward CO and H_2 after 1, 2, and 3 days.

Table 1. Summary of Cumulative Solar-to-Chemical Efficiencies and *STC* toward CO and H_2 after 1, 2, and 3 days

STC, %	STC H_2, %	STC CO, %	days
10.50 ± 0.03	1.70 ± 0.01	8.80 ± 0.02	1 day
10.5	2.3	8.2	2 days
10.2	2.4	7.8	3 days

The *STC* decreased from 10.5% on day 1 to 10.2% on day 3, mainly due to a lower total faradaic efficiency of the collected products. Although CO remained dominant, its selectivity was the lowest on day 3. On days 1 and 2, the decrease in CO selectivity is counterbalanced by an increase in H_2 selectivity. Day 1 was repeated in 3 independent experiments.

The STC_{CO} decay under constant voltage operation (V_{OP} of 3.0 V) is presented in the Supporting Information, Figures S8 and S9. For comparison, we ensure that in both cases, the same total charge was passed, 2359.6 mA·h. Under dynamic operations, the STC_{CO} values decreased from 8.8 to 8.2% from day 1 to day 2. Under constant voltage conditions, the system maintains STC_{CO} values between 8.3 and 8.4%, owing to the stable CO faradaic efficiency. On the first day under dynamic operation, PV-EC benefits from low V_{OP} at the beginning and end of the simulated day, with very high CO selectivity for most part of the day. However, on day 2, the overall CO selectivity decreased. Additionally, Figure S10 in the Supporting Information presents the static CO_2RR performance at potentials ranging from 2.4 to 3.4 V, expressed in terms of faradaic efficiency. Whether powered by PV or by a source measurement unit at different potentials, the CO_2RR consistently achieves a high CO selectivity.

The reported STC_{CO} efficiencies improved from 6 to 19% due to advances in CO_2RR catalysts,[41−46] EC design, and notably, PV efficiency. Comparing PV-EC systems[5,47−58] requires accounting for PV performance, as shown in Figure 3, which plots STC_{CO} versus PV efficiency. High STC_{CO} values (13−20%) are typically achieved with high-efficiency PVs like GaInP/GaInAs/Ge or GaAs (PV efficiency above 28%) and are mostly used in concentrator photovoltaics (CPV).[52−57,59] However, their cost, complexity, and limited performance under diffuse light hinder broad adoption. Silicon-based PV remains the dominant and scalable choice, making it the most practical option for coupling with CO_2 electrolysis systems.

Si−PV connected to CO_2RR flow-type EC devices shows typical STC_{CO} between 2.5 and 8%.[5,50,51] Herein, we report a notable cumulative STC_{CO} efficiency of 8.8% after day 1, 8.2 and 7.8% after day 2 and day 3, respectively, using silver nanoparticle GDE. Furthermore, in realistic scenarios, PV-EC systems operate across low to high current densities daily. A high-performance cathode should maintain a stable STC_{CO} over this range. In this study, Ag-GDE in flow-type EC directly connected to emulated Si-PV promotes high and stable STC_{CO}

https://doi.org/10.1021/acs.energyfuels.5c03523
Energy Fuels 2025, 39, 22776−22783

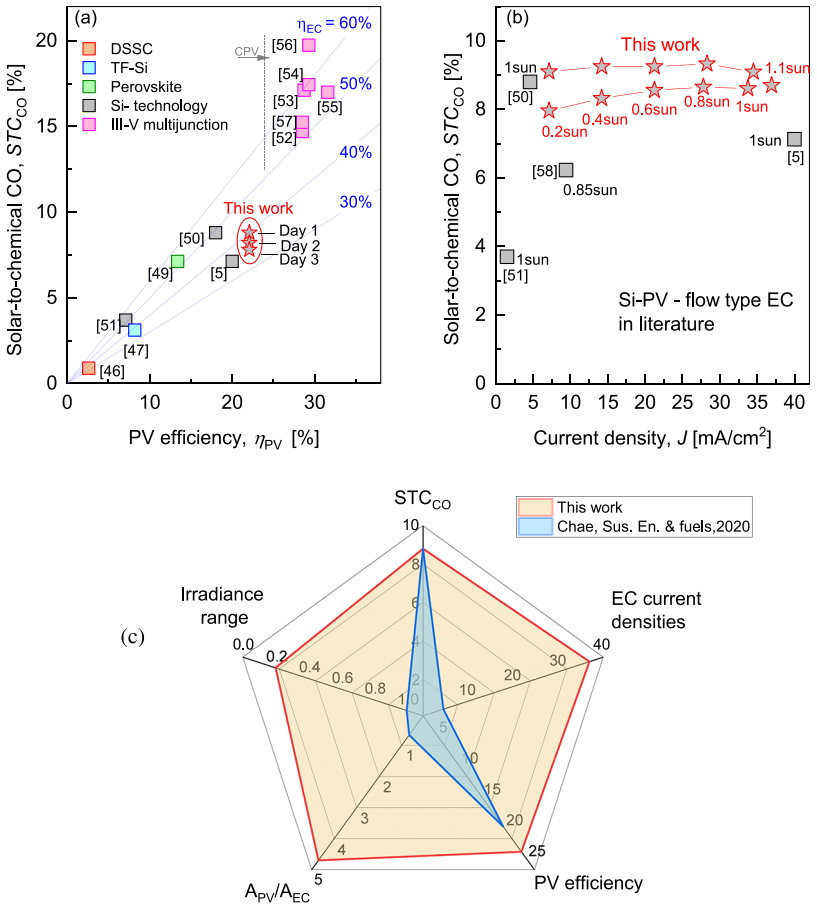

Figure 3. (a) Solar-to-chemical CO efficiency as a function of PV efficiency for different PV technologies. The orange square represents dye-sensitized solar cells (DSSC),[46] The light blue square represents thin-film silicon technology (TF-Si),[47] the green square represents perovskite technology,[49] the gray squares represent Si-technology PV,[5,50,51] and the violet squares represent III−V multijunction PV, used as CPV.[52−57] The blue guidelines represent STC_{CO} evolution plotted against PV efficiency when η_{EC} values, EC efficiency toward CO, are 30, 40, 50 and 60% with a maximum PV-EC power coupling. (b) Solar-to-chemical CO efficiency as a function of current density for reported Si−PV connected to flow-type EC.[5,50,51,58] (c) STC_{CO}, current densities, PV efficiency, PV-to-EC area ratio, and tested irradiances for our Si−PV-EC compared to the best prior results from Chae et al.

across a wide dynamic range of electrolyzer current densities, from 7 mA/cm^2 to 37 mA/cm^2, as illustrated in Figure 3b.

To date, the highest STC_{CO} (8.03%) in Si-PV-flow EC systems was reported by Chae et al. using a nanoporous silver film, where the CO_2 supply was restricted to the fraction dissolved in the electrolyte. The system achieved a CO selectivity of 94% but was limited to low current densities (2−6 mA/cm^2, tested at 4.6 mA/cm^2) and was operated under constant standard conditions of 1 sun.[50] In contrast, our cathode architecture incorporates a gas diffusion electrode that maximizes the interaction between CO_2 molecules and the silver catalyst particles, enabling higher current densities (7−37 mA/cm^2) with high CO faradaic efficiency.

The tested catalyst can be transferred to more industry-relevant advanced zero-gap membrane electrode assembly electrolyzers.[60−62] The Ag-GDE and testing method enabled an accurate assessment of its viability for PV-powered CO_2 reduction under realistic conditions, including dynamic G and T cycling, day−night transitions, a wide current density range, and a high PV-to-EC area ratio (4.7). Figure 3c illustrates the operational context and STC_{CO} of PV-EC (with silver nanoporous film cathode) from the best prior result by Chae et al.,[50] compared with the broader investigation scope and STC_{CO} (on day 1) achieved in this work with Ag-GDE.

To the best of our knowledge, the cumulative STC_{CO} values after day 1 (8.8%) and day 2 (8.2%) are the highest reported for Si-PV-flow-type EC class devices for current densities above 4.6 mA/cm^2.

3. CONCLUSIONS

In summary, although CO_2 reduction catalysts have shown improved stability and selectivity, they are usually tested under steady-state conditions or within narrow voltage−current ranges. PV-powered EC devices for the CO_2RR offer high solar-to-chemical efficiency under fixed, standard lab conditions. However, the real PV output fluctuates with solar irradiance and temperature, requiring performance assessments under realistic, variable conditions. CO_2RR catalysts must tolerate intermittent power while ensuring consistent product output across a broad dynamic range. This study demonstrates the viability of a silver-based gas diffusion electrode (Ag-GDE) for CO_2 reduction in a directly coupled PV-EC system operating under realistic fluctuating solar conditions. The Ag-GDE, integrated into a full-flow EC cell with an iridium oxide anode, maintained stable CO selectivity and high energy coupling efficiency (0.96) across three day/night cycles emulated from the real Si-PV output. The system achieved cumulative solar-to-chemical efficiencies (STC_{CO}) of 8.8, 8.2,

https://doi.org/10.1021/acs.energyfuels.5c03523
Energy Fuels 2025, 39, 22776−22783

and 7.8%, the highest reported for Si-PV-driven flow EC devices across a broad current density range (7−37 mA/cm^2). This is the first demonstration of such performance under realistic dynamic conditions, highlighting the promise of Ag-GDE for efficient, stable, and scalable PV-powered CO_2 conversion.

■ ASSOCIATED CONTENT

Supporting Information

The Supporting Information is available free of charge at https://pubs.acs.org/doi/10.1021/acs.energyfuels.5c03523.

Effects of irradiance and temperature on PV current−voltage characteristics; PV-EC dynamic operation under realistic ambient conditions during a nonaccelerated day; PV-EC dynamic operation under realistic ambient conditions during a highly accelerated day; Ag-GDE characterization before and after the test; EDX maps of the post-test Ag-GDE cross section; electrochemical cell stability and frequency of electrolyte refill study; comparison of PV-EC operating in static and dynamic modes; preparation of silver gas diffusion electrode, CO_2RR experiment, and PV-EC experiment with PV emulation; irradiance and temperature realistic ambient conditions; and PV-EC system efficiency evaluation (PDF)

■ AUTHOR INFORMATION

Corresponding Author

Tsvetelina Merdzhanova − *Forschungszentrum Jülich GmbH, IMD-3 Photovoltaik, Jülich 52428, Germany;* orcid.org/0000-0003-0902-6330; Email: t.merdzhanova@fz-juelich.de

Authors

Thérèse Cibaka − *Forschungszentrum Jülich GmbH, IMD-3 Photovoltaik, Jülich 52428, Germany; Technical University of Berlin, Institute of Chemistry, Berlin 10623, Germany*

Oleksandr Astakhov − *Forschungszentrum Jülich GmbH, IMD-3 Photovoltaik, Jülich 52428, Germany;* orcid.org/0000-0001-8499-058X

Sergey Shcherbachenko − *Forschungszentrum Jülich GmbH, IMD-3 Photovoltaik, Jülich 52428, Germany; Jülich Aachen Research Alliance (JARA-Energy) and Faculty of Electrical Engineering and Information Technology, RWTH Aachen University, Aachen 52062, Germany*

Guangxin Liu − *Helmholtz-Institute Erlangen-Nürnberg for Renewable Energy (IET-2), Erlangen 91058, Germany*

Chuyen van Pham − *Helmholtz-Institute Erlangen-Nürnberg for Renewable Energy (IET-2), Erlangen 91058, Germany*

Uwe Rau − *Forschungszentrum Jülich GmbH, IMD-3 Photovoltaik, Jülich 52428, Germany; Jülich Aachen Research Alliance (JARA-Energy) and Faculty of Electrical Engineering and Information Technology, RWTH Aachen University, Aachen 52062, Germany*

Peter Strasser − *Technical University of Berlin, Institute of Chemistry, Berlin 10623, Germany;* orcid.org/0000-0002-3884-436X

Complete contact information is available at: https://pubs.acs.org/10.1021/acs.energyfuels.5c03523

Notes

The authors declare no competing financial interest.

■ ACKNOWLEDGMENTS

The authors would like to thank Joachim Kirchhoff and Daniel Weigand for their technical support in building the CO_2 reduction setup, Ugochi Chime for the Silicon heterojunction PV cell preparation and $I-V$ curve measurements, and Lars Wieprecht for the daily laboratory support. This work made use of the Research Center Juelich facilities, and the authors express gratitude to the HITEC program for funding. The authors gratefully acknowledge the European Commission under the DECADE and SUPERVAL Projects (Grant agreements no: 862030 and 101115456, respectively).

■ REFERENCES

(1) IRENA. Renewable energy statistics 2024, International Renewable Energy Agency, Abu Dhabi. IRENA 2024 https://www.irena.org/-/media/Files/IRENA/Agency/Publication/2024/Jul/IRENA_Renewable_Energy_Statistics_2024.pdf (accessed May 12, 2025).

(2) Bojek, P. Energy-system/Renewables/Solar-pv 2023 https://www.iea.org/energy-system/renewables/solar-pv.

(3) Burdyny, T.; Smith, W. A. CO2 reduction on gas-diffusion electrodes and why catalytic performance must be assessed at commercially-relevant conditions. *Energy Environ. Sci.* **2019**, *12* (5), 1442−1453.

(4) Luan, C.; Shao, Y.; Lu, Q.; Gao, S.; Huang, K.; Wu, H.; Yao, K. High-Performance Carbon Dioxide Electrocatalytic Reduction by Easily Fabricated Large-Scale Silver Nanowire Arrays. *ACS Appl. Mater. Interfaces* **2018**, *10* (21), 17950−17956.

(5) Sriramagiri, G. M.; Ahmed, N.; Luc, W.; Dobson, K. D.; Hegedus, S. S.; Jiao, F. Toward a Practical Solar-Driven CO2 Flow Cell Electrolyzer: Design and Optimization. *ACS Sustainable Chem. Eng.* **2017**, *5* (11), 10959−10966.

(6) Shcherbachenko, S.; Astakhov, O.; Chime, U.; Kin, L.-C.; Ding, K.; Pieters, B.; Rau, U.; Figgemeier, E.; Merdzhanova, T. Efficient Power Coupling in Directly Connected Photovoltaic-Battery Module. *Solar RRL* **2023**, *7* (3), 2200857−2200865.

(7) Chibuko, U.; Merdzhanova, T.; Weigand, D.; Ezema, F.; Agbo, S.; Rau, U.; Astakhov, O. Module-level direct coupling in PV-battery power unit under realistic irradiance and load. *Sol. Energy* **2023**, *249*, 233−241.

(8) Lee, M.; Ding, X.; Banerjee, S.; Krause, F.; Smirnov, V.; Astakhov, O.; Merdzhanova, T.; Klingebiel, B.; Kirchartz, T.; Finger, F.; et al. Bifunctional CoFeVOx Catalyst for Solar Water Splitting by using Multijunction and Heterojunction Silicon Solar Cells. *Adv. Mater. Technol.* **2020**, *5* (12), 2000592−2200601.

(9) Ampelli, C.; Giusi, D.; Miceli, M.; Merdzhanova, T.; Smirnov, V.; Chime, U.; Astakhov, O.; Martín, A. J.; Veenstra, F. L. P.; Pineda, F. A. G.; et al. An artificial leaf device built with earth-abundant materials for combined H2 production and storage as formate with efficiency >10%. *Energy Environ. Sci.* **2023**, *16* (4), 1644−1661.

(10) Astakhov, O.; Agbo, S. N.; Welter, K.; Smirnov, V.; Rau, U.; Merdzhanova, T. Storage batteries in photovoltaic−electrochemical device for solar hydrogen production. *J. Power Sources* **2021**, *509*, No. 230367.

(11) Kin, L.-C.; Astakhov, O.; Lee, M.; Haas, S.; Ding, K.; Merdzhanova, T.; Rau, U. Batteries to keep solar driven water splitting running at night: Performance of a directly coupled system. *Solar RRL* **2022**, *6*, No. 2100916, DOI: 10.1002/solr.202100916.

(12) Phan Van, L.; Hieu Hoang, L.; Nguyen Duc, T. A comprehensive review of direct coupled photovoltaic-electrolyser system: Sizing techniques, operating strategies, research progress, current challenges, and future recommendations. *Int. J. Hydrogen Energy* **2023**, *48* (65), 25231−25249.

(13) Clarke, R. E.; Giddey, S.; Ciacchi, F. T.; Badwal, S. P. S.; Paul, B.; Andrews, J. Direct coupling of an electrolyser to a solar PV system for generating hydrogen. *Int. J. Hydrogen Energy* **2009**, *34* (6), 2531−2542.

(14) Chang, W. J.; Lee, K. H.; Ha, H.; Jin, K.; Kim, G.; Hwang, S. T.; Lee, H. M.; Ahn, S. W.; Yoon, W.; Seo, H.; et al. Design Principle and Loss Engineering for Photovoltaic-Electrolysis Cell System. *ACS Omega* **2017**, *2* (3), 1009−1018.
(15) Jia, J.; Seitz, L. C.; Benck, J. D.; Huo, Y.; Chen, Y.; Ng, J. W.; Bilir, T.; Harris, J. S.; Jaramillo, T. F. Solar water splitting by photovoltaic-electrolysis with a solar-to-hydrogen efficiency over 30. *Nat. Commun.* **2016**, *7*, No. 13237.
(16) Gurudayal, G.; Bullock, J.; Srankó, D. F.; Towle, C. M.; Lum, Y.; Hettick, M.; Scott, M. C.; Javey, A.; Ager, J. Efficient solar-driven electrochemical CO2 reduction to hydrocarbons and oxygenates. *Energy Environ. Sci.* **2017**, *10* (10), 2222−2230.
(17) Park, H.; Park, I. J.; Lee, M. G.; Kwon, K. C.; Hong, S. P.; Kim, D. H.; Lee, S. A.; Lee, T. H.; Kim, C.; Moon, C. W.; et al. Water Splitting Exceeding 17% Solar-to-Hydrogen Conversion Efficiency Using Solution-Processed Ni-Based Electrocatalysts and Perovskite/Si Tandem Solar Cell. *ACS Appl. Mater. Interfaces* **2019**, *11* (37), 33835−33843.
(18) Beiler, A. M.; Li, W.; Denisiuk, A.; Palomares, E.; Llobet, A. Solar hydrogen production from electrochemical ammonia splitting powered by a single perovskite solar cell. *J. Energy Chem.* **2024**, *92*, 292−295.
(19) Heremans, G.; Trompoukis, C.; Daems, N.; Bosserez, T.; Vankelecom, I. F. J.; Martens, J. A.; Rongé, J. Vapor-fed solar hydrogen production exceeding 15% efficiency using earth abundant catalysts and anion exchange membrane. *Sustainable Energy Fuels* **2017**, *1* (10), 2061−2065.
(20) Reuß, M.; Reul, J.; Grube, T.; Langemann, M.; Calnan, S.; Robinius, M.; Schlatmann, R.; Rau, U.; Stolten, D. Solar hydrogen production: a bottom-up analysis of different photovoltaic−electrolysis pathways. *Sustainable Energy Fuels* **2019**, *3* (3), 801−813.
(21) Astakhov, O.; Merdzhanova, T.; Kin, L.-C.; Rau, U. From room to roof: How feasible is direct coupling of solar-battery power unit under variable irradiance? *Sol. Energy* **2020**, *206*, 732−740.
(22) Schüttauf, J.-W.; Modestino, M. A.; Chinello, E.; Lambelet, D.; Delfino, A.; Dominé, D.; Faes, A.; Despeisse, M.; Bailat, J.; Psaltis, D.; et al. Solar-to-Hydrogen Production at 14.2% Efficiency with Silicon Photovoltaics and Earth-Abundant Electrocatalysts. *J. Electrochem. Soc.* **2016**, *163* (10), F1177−F1181.
(23) Merten, J.; Asensi, J. M.; Voz, C.; Shah, A. V.; Platz, R.; Andreu, J. Improved equivalent circuit and analytical model for amorphous silicon solar cells and modules. *IEEE Trans. Electron Devices* **1998**, *45* (2), 423−429.
(24) Agbo, S. N.; Merdzhanova, T.; Rau, U.; Astakhov, O. Illumination intensity and spectrum-dependent performance of thin-film silicon single and multijunction solar cells. *Sol. Energ Mat. Sol. C* **2017**, *159*, 427−434.
(25) Bunea, G. E.; Wilson, K. E.; Meydbray, Y.; Campbell, M. P.; Ceuster, D. M. D. *Low Light Performance of Mono-Crystalline Silicon Solar Cells*, 2006 IEEE 4th World Conference on Photovoltaic Energy Conference, Vol. 2, 2006; pp 1312−1314 (May 7−12, 2006).
(26) Bahrami-Yekta, V.; Tiedje, T. Limiting efficiency of indoor silicon photovoltaic devices. *Opt. Express* **2018**, *26* (22), 28238−28248.
(27) Dupré, O.; Vaillon, R.; Green, M. A.Thermal Behavior of Photovoltaic Devices. 2017 DOI: 10.1007/978-3-319-49457-9.
(28) Jordaan, S. M.; Wang, C. Electrocatalytic conversion of carbon dioxide for the Paris goals. *Nat. Catal.* **2021**, *4* (11), 915−920.
(29) Liu, G. X.; McLaughlin, D.; Thiele, S.; Van Pham, C. Correlating catalyst ink design and catalyst layer fabrication with electrochemical CO2 reduction performance. *Chem. Eng. J.* **2023**, *460*, 141757−141770.
(30) Liu, J.; Yang, Y.; Petit, E.; Bonniol, V.; Anfar, Z.; Rebiere, B.; Karamoko, B. A.; Wang, W.; Wu, H.; Moderne, M.; et al. Structural Insights into Ni−Fe Layered Double Hydroxides as Anode Catalysts for Pairing CO2 Reduction and Ethylene Glycol Oxidation. *ACS Catal.* **2025**, *15*, 11861−11874.
(31) Seidler, M. F.; Pieters, B.; Zwaygardt, W.; Haas, S.; Astakhov, O.; Merdzhanova, T. A photovoltaics emulator for electrochemistry using Python and SCPI. *J. Power Sources* **2025**, *641*, No. 236723.
(32) Marion, B.; Deceglie, M. G.; Silverman, T. J. Analysis of measured photovoltaic module performance for Florida, Oregon, and Colorado locations. *Sol. Energy* **2014**, *110*, 736−744.
(33) Krishnan, S.; Koning, V.; Theodorus de Groot, M.; de Groot, A.; Mendoza, P. G.; Junginger, M.; Kramer, G. J. Present and future cost of alkaline and PEM electrolyser stacks. *Int. J. Hydrogen Energy* **2023**, *48* (83), 32313−32330.
(34) Hallam, B.; Kim, M.; Zhang, Y.; Wang, L.; Lennon, A.; Verlinden, P.; Altermatt, P. P.; Dias, P. R. The silver learning curve for photovoltaics and projected silver demand for net-zero emissions by 2050. *Prog. Photovoltaics* **2023**, *31* (6), 598−606.
(35) Shcherbachenko, S.; Astakhov, O.; Chime, U.; Kin, L.-C.; Ding, K.; Pieters, B.; Rau, U.; Figgemeier, E.; Merdzhanova, T. Efficient Power Coupling in Directly Connected Photovoltaic-Battery Module. *Solar RRL* **2023**, *7* (3), 2200857−2200865.
(36) Valenti, M.; Prasad, N. P.; Kas, R.; Bohra, D.; Ma, M.; Balasubramanian, V.; Chu, L.; Gimenez, S.; Bisquert, J.; Dam, B.; Smith, W. A. Suppressing H2 Evolution and Promoting Selective CO2 Electroreduction to CO at Low Overpotentials by Alloying Au with Pd. *ACS Catal.* **2019**, *9* (4), 3527−3536.
(37) Hsieh, Y.-C.; Senanayake, S. D.; Zhang, Y.; Xu, W.; Polyansky, D. E. Effect of Chloride Anions on the Synthesis and Enhanced Catalytic Activity of Silver Nanocoral Electrodes for CO2 Electroreduction. *ACS Catal.* **2015**, *5* (9), 5349−5356.
(38) Ma, M.; Trześniewski, B. J.; Xie, J.; Smith, W. A. Selective and Efficient Reduction of Carbon Dioxide to Carbon Monoxide on Oxide-Derived Nanostructured Silver Electrocatalysts. *Angew. Chem., Int. Ed.* **2016**, *55* (33), 9748−9752.
(39) Krause, K.; Lee, J. K.; Lee, C.; Shafaque, H. W.; Kim, P. J.; Fahy, K. F.; Shrestha, P.; LaManna, J. M.; Baltic, E.; Jacobson, D. L.; et al. Electrolyte layer gas triggers cathode potential instability in CO2 electrolyzers. *J. Power Sources* **2022**, *520*, No. 230879.
(40) Ampelli, C.; Tavella, F.; Giusi, D.; Ronsisvalle, A. M.; Perathoner, S.; Centi, G. Electrode and cell design for CO2 reduction: A viewpoint. *Catal. Today* **2023**, *421*, No. 114217.
(41) Li, Y. C.; Lee, G.; Yuan, T.; Wang, Y.; Nam, D.-H.; Wang, Z.; García de Arquer, F. P.; Lum, Y.; Dinh, C.-T.; Voznyy, O.; Sargent, E. H. CO2 Electroreduction from Carbonate Electrolyte. *ACS Energy Lett.* **2019**, *4* (6), 1427−1431.
(42) Goh, D. Y. Y.; Yam, K. M.; Rekhi, L.; Handoko, A. D.; Tan, Y. C.; Wang, Y.; Tan, J. M. R.; Choksi, T. S.; Lum, Y.; Wong, L. H. Covalency-aided electrochemical CO2 reduction to CO on sulfide-derived Cu−Sb. *J. Mater. Chem. A* **2024**, *12* (3), 1840−1851.
(43) Wu, B.; Voleti, L. D.; Fenwick, A. Q.; Wu, C.; Zhang, J.; Ling, N.; Wang, M.; Jia, Y.; Tjiu, W. W.; Zhang, M.; et al. A reversed gas diffusion electrode enables collection of high purity gas products from CO2 electroreduction. *EES Catal.* **2025**, *3*, 318−326.
(44) Sarma, S. C.; Barrio, J.; Bagger, A.; Pedersen, A.; Gong, M.; Luo, H.; Wang, M.; Favero, S.; Zhao, C.-X.; Zhang, Q.; et al. Reaching the Fundamental Limitation in CO2 Reduction to CO with Single Atom Catalysts. *Adv. Funct. Mater.* **2023**, *33* (41), No. 2302468.
(45) Yang, S.; Liu, Z.; An, H.; Arnouts, S.; de Ruiter, J.; Rollier, F.; Bals, S.; Altantzis, T.; Figueiredo, M. C.; Filot, I. A. W.; et al. Near-Unity Electrochemical CO2 to CO Conversion over Sn-Doped Copper Oxide Nanoparticles. *ACS Catal.* **2022**, *12* (24), 15146−15156.
(46) Lyu, X.; Anastasiadou, D.; Raj, J.; Wu, J.; Bai, Y.; Li, J.; Cullen, D. A.; Yang, J.; Gonçalves, L. P. L.; Lebedev, O. I.; et al. Large-scale synthesis of metal/nitrogen Co-doped carbon catalysts for CO2 electroreduction. *Electrochim. Acta* **2023**, *455*, No. 142427.
(47) Sacco, A.; Speranza, R.; Savino, U.; Zeng, J.; Farkhondehfal, M. A.; Lamberti, A.; Chiodoni, A.; Pirri, C. F. An Integrated Device for the Solar-Driven Electrochemical Conversion of CO2 to CO. *ACS Sustainable Chem. Eng.* **2020**, *8* (20), 7563−7568.
(48) Veenstra, F. L. P.; Cibaka, T.; Martin, A. J.; Weigand, D.; Kirchhoff, J.; Smirnov, V.; Merdzhanova, T.; Perez-Ramirez, J. CO(2)

Electroreduction To Syngas With Tunable Composition In An Artificial Leaf. *ChemSusChem* **2024**, *17* (4), No. e202301398.
(49) Schreier, M.; Curvat, L.; Giordano, F.; Steier, L.; Abate, A.; Zakeeruddin, S. M.; Luo, J.; Mayer, M. T.; Grätzel, M. Efficient photosynthesis of carbon monoxide from CO2 using perovskite photovoltaics. *Nat. Commun.* **2015**, *6*, No. 7326.
(50) Chae, S. Y.; Lee, S. Y.; Han, S. G.; Kim, H.; Ko, J.; Park, S.; Joo, O. S.; Kim, D.; Kang, Y.; Lee, U.; et al. A perspective on practical solar to carbon monoxide production devices with economic evaluation. *Sustainable Energy Fuels* **2020**, *4* (1), 199−212.
(51) Arai, T.; Sato, S.; Sekizawa, K.; Suzuki, T. M.; Morikawa, T. Solar-driven CO2 to CO reduction utilizing H2O as an electron donor by earth-abundant Mn−bipyridine complex and Ni-modified Fe-oxyhydroxide catalysts activated in a single-compartment reactor. *Chem. Commun.* **2019**, *55* (2), 237−240.
(52) Schreier, M.; Héroguel, F.; Steier, L.; Ahmad, S.; Luterbacher, J. S.; Mayer, M. T.; Luo, J.; Grätzel, M. Solar conversion of CO2 to CO using Earth-abundant electrocatalysts prepared by atomic layer modification of CuO. *Nat. Energy* **2017**, *2* (7), No. 17087.
(53) Wang, Y.; Liu, J.; Wang, Y.; Wang, Y.; Zheng, G. Efficient solar-driven electrocatalytic CO2 reduction in a redox-medium-assisted system. *Nat. Commun.* **2018**, *9* (1), No. 5003.
(54) Kim, B.; Seong, H.; Song, J. T.; Kwak, K.; Song, H.; Tan, Y. C.; Park, G.; Lee, D.; Oh, J. Over a 15.9% Solar-to-CO Conversion from Dilute CO2 Streams Catalyzed by Gold Nanoclusters Exhibiting a High CO2 Binding Affinity. *ACS Energy Lett.* **2020**, *5* (3), 749−757.
(55) Mi, Y.; Qiu, Y.; Liu, Y.; Peng, X.; Hu, M.; Zhao, S.; Cao, H.; Zhuo, L.; Li, H.; Ren, J.; et al. Cobalt−Iron Oxide Nanosheets for High-Efficiency Solar-Driven CO2−H2O Coupling Electrocatalytic Reactions. *Adv. Funct. Mater.* **2020**, *30* (31), No. 2003438.
(56) Cheng, W.-H.; Richter, M. H.; Sullivan, I.; Larson, D. M.; Xiang, C.; Brunschwig, B. S.; Atwater, H. A. CO2 Reduction to CO with 19% Efficiency in a Solar-Driven Gas Diffusion Electrode Flow Cell under Outdoor Solar Illumination. *ACS Energy Lett.* **2020**, *5* (2), 470−476.
(57) Zhou, L. Q.; Ling, C.; Zhou, H.; Wang, X.; Liao, J.; Reddy, G. K.; Deng, L.; Peck, T. C.; Zhang, R.; Whittingham, M. S.; et al. A high-performance oxygen evolution catalyst in neutral-pH for sunlight-driven CO2 reduction. *Nat. Commun.* **2019**, *10* (1), No. 4081.
(58) Xu, K.; Ning, S.; Chen, H.; Ouyang, S.; Wang, J.; Song, L.; Lv, J.; Ye, J. Plum Pudding-Like Electrocatalyst of N-Doped SnO@Sn Loaded on Carbon Matrix to Construct Photovoltaic CO2 Reduction System with Solar-to-Fuel Efficiency of 11.3%. *Solar RRL* **2020**, *4* (7), No. 2000116.
(59) Wang, X.; Ghausi, M. A.; Yang, R.; Wu, M.; Xie, J.; Wang, Y. A photovoltaic-driven solid-state Zn−CO2 electrochemical cell system with sunlight-insusceptible chemical production. *J. Mater. Chem. A* **2020**, *8* (27), 13806−13811.
(60) Hoof, L.; Thissen, N.; Pellumbi, K.; junge Puring, K.; Siegmund, D.; Mechler, A. K.; Apfel, U.-P. Hidden parameters for electrochemical carbon dioxide reduction in zero-gap electrolyzers. *Cell Rep. Phys. Sci.* **2022**, *3* (4), No. 100825.
(61) Sassenburg, M.; Kelly, M.; Subramanian, S.; Smith, W. A.; Burdyny, T. Zero-Gap Electrochemical CO2 Reduction Cells: Challenges and Operational Strategies for Prevention of Salt Precipitation. *ACS Energy Lett.* **2023**, *8* (1), 321−331.
(62) Goldman, M.; Krall, E.; Marufu, M.; Jue, M. L.; Tzintzun, S.; Wagner, J. K.; Jaffer, S.; Sarkar, A.; Fleischer, M.; Simon, E.; et al. Integration of hydrophobic gas diffusion layers for zero-gap electrolyzers to enable highly energy-efficient CO2 electrolysis to C2 products. *Chem. Catal.* **2025**, *5*, No. 101235.

https://doi.org/10.1021/acs.energyfuels.5c03523
Energy Fuels 2025, 39, 22776−22783